Electrochemical Deposition of Copper(I) Oxide Films

Teresa D. Golden, Mark G. Shumsky, Yanchun Zhou, Rachel A. VanderWerf, Robert A. Van Leeuwen, and Jay A. Switzer*

Department of Chemistry and Graduate Center for Materials Research, University of Missouri—Rolla, Rolla, Missouri 65409-1170

Received April 3, 1996. Revised Manuscript Received June 19, 1996[⊗]

Films of copper(I) oxide can be electrodeposited by reduction of copper(II) lactate in alkaline solution. Rietveld analysis of electrochemically grown films reveals pure copper(I) oxide with no copper(II) oxide or copper metal present in the films and a lattice parameter of $a = 0.4266$ nm. The cathodic deposition current is limited by a Schottky-like barrier that forms between the Cu_2O and the deposition solution. A barrier height of 0.6 eV was determined from the exponential dependence of the deposition current on the solution temperature. At a solution pH of 9 the orientation of the film is [100], while at a solution pH of 12 the orientation changes to [111]. Atomic force images of the [100] oriented films have crystals shaped as four-sided pyramids, while the [111] films have triangular crystals. The grain size for films grown at 65 °C ranges from 2 to 5 μm. A refractive index of 2.6 was measured from the transmission spectrum for wavelengths between 1350 and 2800 nm. The p-type semiconductor has a direct bandgap of 2.1 eV.

Introduction

Electrochemistry is an attractive technique for materials synthesis. Electrodeposition can be used to deposit a variety of materials such as ceramics,[1−4] semiconductors,[5] superlattices,[6,7] and superconductors.[8] A wide range of semiconductors have been electrodeposited including quantum dots of CdSe,[9] epitaxial films of CdTe on InP,[10] and epitaxial layers of GaAs.[11]

The emphasis in our laboratory is on electrodeposition of metal oxide ceramics. We have previously shown that it is possible to electrochemically prepare CeO_2,[4,12] ZrO_2,[13] AgO,[14] $Ag(Ag_3O_4)_2NO_3$,[3] and both compositional[1,6,15] and defect chemistry[7] superlattices. In the present work we extend the electrodeposition technique to a metal oxide ceramic which is also a semiconductor. Our motivation is 2-fold: First, we are interested in electrodepositing nanoscale materials in the form of superlattices and nanocomposites. Since the oxide is a semiconductor, we are more likely to observe quantum confinement effects such as bandgap blue-shifting when the dimensions approach the nanometer scale. Our previously deposited superlattices were highly conducting metal oxide degenerate semiconductors,[16] in which quantum confinement of carriers is not likely. The other motivation for depositing copper(I) oxide is that we wish to gain experience in the deposition of copper oxides for the possible electrodeposition of copper oxide superconductors.

Copper(I) oxide (Cu_2O) is a p-type semiconductor with reported resistivity varying from a few Ω cm to 10^{14} Ω cm, depending on the preparation technique. Techniques for making Cu_2O include thermal oxidation,[17,18] chemical oxidation,[19] anodic oxidation,[20] and vacuum evaporation.[21,22] Cu_2O has also been electrochemically deposited onto several substrates.[23−26] Electrochemical deposition of films offers precise control of the driving force for the reactions involved in deposition, allowing control of the structure and phase composition of the films. In this paper we report some preliminary electrochemical, X-ray, and optical results for Cu_2O films which we electrodeposited from an aqueous solution.

Experimental Section

The electrochemical deposition of Cu_2O films was conducted in an electrolyte solution consisting of 0.4 M cupric sulfate

* To whom correspondence should be addressed.

[⊗] Abstract published in *Advance ACS Abstracts,* August 15, 1996.

(1) Switzer, J. A.; Shane, M. J.; Phillips, R. J. *Science* **1990**, *247*, 444.
(2) Feng, J.; Johnson, D. C. *J. Electrochem. Soc.* **1990**, *137*, 506.
(3) Breyfogle, B. E.; Phillips, R. J.; Switzer, J. A. *Chem. Mater.* **1992**, *4*, 1356.
(4) Switzer, J. A. *Am. Ceram. Soc. Bull.* **1987**, *66*, 1521.
(5) Rajeshwar, K. *Adv. Mater.* **1992**, *4*, 23.
(6) Switzer, J. A.; Raffaelle, R. P.; Phillips, R. J.; Hung, C. J.; Golden, T. D. *Science* **1992**, *258*, 1918.
(7) Switzer, J. A.; Hung, C. J.; Breyfogle, B. E.; Shumsky, M. G.; Van Leeuwen, R.; Golden, T. D. *Science* **1994**, *264*, 1573.
(8) Norton, M. L. *Mater. Res. Bull.* **1989**, *24*, 1391.
(9) Golan, Y.; Margulis, L.; Hodes, G.; Rubinstein, I.; Hutchison, J. L. *Surf. Sci.* **1994**, *311*, L633.
(10) Lincot, D.; Kampmann, A.; Mokili, B.; Vedel, J.; Cortes, R.; Froment, M. *Appl. Phys. Lett.* **1995**, *67*, 2355.
(11) Villegas, I.; Stickney, J. L. *J. Electrochem. Soc.* **1992**, *139*, 686.
(12) Zhou, Y.; Phillips, R. J.; Switzer, J. A. *J. Am. Ceram. Soc.* **1995**, *78*, 981.
(13) Switzer, J. A.; Phillips, R. J. *Mater. Res. Soc. Symp. Proc.* **1988**, *121*, 111.
(14) Breyfogle, B. E.; Hung, C. J.; Shumsky, M. G.; Switzer, J. A. *J. Electrochem. Soc.* **1996**, *143*, 2741.
(15) Switzer, J. A.; Golden, T. D. *Adv. Mater.* **1993**, *5*, 474.
(16) Van Leeuwen, R. A.; Hung, C. J.; Kammler, D. R.; Switzer, J. A. *J. Phys. Chem.* **1995**, *99*, 15247.
(17) Xue, J.; Dieckmann, R. *J. Phys. Chem. Solids* **1990**, *51*, 1263.
(18) Shimizu, K.; Kobayashi, K.; Thompson, G. E.; Wood, G. C. *Corros. Sci.* **1994**, *36*, 621.
(19) Ristov, M.; Sinadinovski, G. J.; Mitreski, M. *Thin Solid Films* **1988**, *167*, 309.
(20) Ashworth, V.; Fairhurst, D. *J. Electrochem. Soc.* **1977**, *124*, 506.
(21) Ortiz, C.; Afonso, C. N.; Vega, F.; Solis, J.; Cheang, J. C.; Ortega, C.; Siejka, J. *Appl. Surf. Sci.* **1992**, *54*, 201.
(22) Özer, N.; Tepehen, F. *Sol. Energy Mater.* **1993**, *30*, 13.
(23) Mukhopadhyay, A. K.; Chakraborty, A. K.; Chatterjee, A. P.; Lahiri, S. K. *Thin Solid Films* **1992**, *209*, 92.
(24) Chatterjee, A. P.; Mukhopadhyay, A. K.; Chakraborty, A. K.; Sasmal, R. N.; Lahiri, S. K. *Mater. Lett.* **1991**, *11*, 358.
(25) Rakhshani, A. E.; Varghese, J. *Thin Solid Films* **1988**, *157*, 87.
(26) Tench, D.; Warren, L. F. *J. Electrochem. Soc.* **1983**, *130*, 869.

S0897-4756(96)00209-8 CCC: $12.00

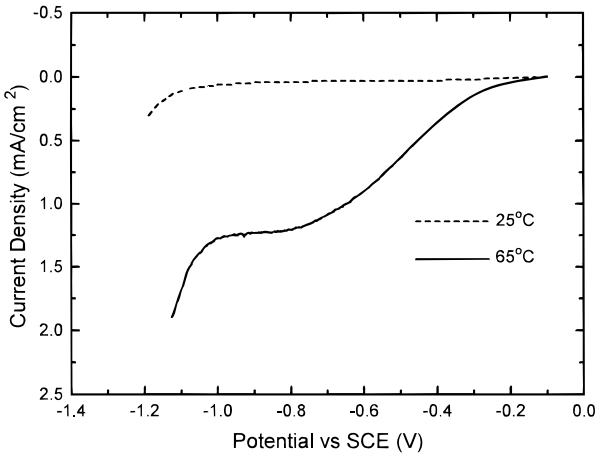

Figure 1. Linear sweep voltammogram at 25 and 65 °C for a 10 μm Cu_2O film deposited at −0.45 V on a stainless steel electrode. Scan rate = 10 mV/s.

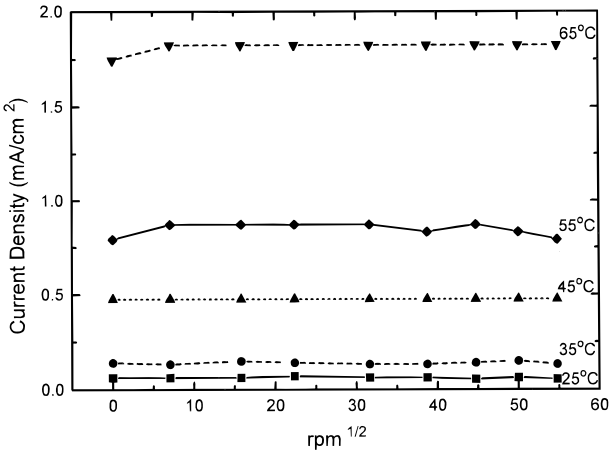

Figure 2. Levich plots for a 10 μm Cu_2O film deposited at −0.45 V.

(Aldrich) and 3 M lactic acid (Aldrich).[27] By complexing with lactate ion, the copper is stabilized and the pH can be raised to alkaline values. The pH of the solution was adjusted between 9 and 12 by the addition of sodium hydroxide (Aldrich). The solution temperature was kept constant during deposition by a Fisher Scientific Model 9100 circulator. Deposition temperatures ranged from 25 to 65 °C. Films were deposited onto either stainless steel or ITO (indium tin oxide) substrates, which were placed in solution with a copper wire counter electrode and a $Cu/CuSO_4$ (0.1 M) reference electrode. All potentials are reported versus the SCE reference electrode. Electrochemical deposition was controlled by an EG&G PAR 273A potentiostat. Data acquisition was obtained by either a 486 PC or a Nicolet Pro 10 oscilloscope.

The structure and phase composition of the films and powders were identified by X-ray diffraction analysis using a Scintag 2000 diffractometer with Cu Kα radiation (λ = 0.154 184 nm). For Rietveld analysis,[28] the films were ground to a powder with a mortar and pestle and sifted through a 270 mesh sieve. During X-ray scanning the powder was continuously rotated on the sample holder. Surface morphologies of the oriented films deposited under different experimental conditions were observed by atomic force microscopy with a scanning probe microscope (Digital Nanoscope III). All samples were imaged in air at a scan rate of 0.75 Hz with gold-coated silicon nitride (Si_3N_4) probes purchased from Digital Instruments. Optical transmittance and absolute specular reflectance were measured at wavelengths from λ = 300 to 2800 nm using a Cary 5 spectrophotometer.

Results and Discussion

Voltammetry was used to study cuprous oxide deposition from the prepared solutions. The solution contained lactic acid which complexes with the free copper(II) ions in solution to form $Cu(CH_3CHOHCOO)_2$.[29] The linear sweep voltammograms for deposition onto a Cu_2O prelayer from a cupric lactate solution at pH 9 are shown in Figure 1. The sweep starts at open-circuit potential and is scanned cathodically at 10 mV/s. The steady-state currents for the deposition of Cu_2O are in a potential window between −0.35 and −0.55 V. This 200 mV window corresponds to the Pourbaix diagram for the Cu, Cu_2O, and CuO system.[30] At 25 °C these current densities are quite low (50 $\mu A/cm^2$) for film deposition but increase with increasing temperature to about 1.2 mA/cm^2 at 65 °C. A plateau region is seen in the voltammograms at both temperatures.

The plateau region that occurs in the voltammograms was studied for Cu_2O deposition using a rotating disk electrode. A 10 μm Cu_2O film was deposited at −0.45 V onto stainless steel. At a series of temperatures (25−65 °C) and rotation rates (0−3000 rpm), the current density versus the square root of the rotation speed (Levich plots) was plotted in Figure 2. The series of resulting Levich plots at different temperatures are flat for the Cu_2O prelayer, showing a nondependence of current on rotation speed. Since the current is independent of rotation rate, the deposition of Cu_2O is not under diffusion control. However, there is an exponential increase in current with increasing temperature for the Levich plots.

We attribute the limiting current during cathodic electrodeposition to a Schottky-like rectifying barrier that forms at the semiconductor/solution interface due to an energetic mismatch between the solution potential and the Fermi level of the semiconductor. It is well-known from semiconductor/solution studies that p-type semiconductors form rectifying barriers toward cathodic reactions and n-type semiconductors form rectifying contacts toward anodic reactions.[31] The temperature-dependent limiting current, then, would be analogous to the dark saturation current in a solid-state diode. The large increase in current at potentials negative of about −1.0 V vs SCE would correspond to diode breakdown. Borrowing from the techniques of the solid-state physics community, we have determined the height of the barrier that forms at the semiconductor/solution interface from the temperature dependence of the limiting current, since the current flow should be an activated process. The limiting current as a function of temperature is shown in Table 1. These limiting currents are not a function of the film thickness, suggesting that it is not the resistance of the film which is limiting the current. Following Sze[32] for a solid-state Schottky barrier, the barrier height can be determined from the

(27) Rakhshani, A. E.; Varghese, J. *Sol. Energy Mater.* **1987**, *15*, 237.
(28) Howard, S. A. *RIQAS*, Materials Data, Inc., Livermore, CA, 1994.
(29) Singh, K. D.; Jain, S. C.; Sakore, T. D.; Biswas, A. B. *Z. Kristallogr.* **1975**, *141*, 473.
(30) Pourbaix, M. *Atlas of Electrochemical Equilibria in Aqueous Solutions*; NACE, Houston, TX, 1974.
(31) Bard, A. J.; Faulkner, L. R. *Electrochemical Methods, Fundamentals and Applications;* John Wiley & Sons: New York 1980.
(32) Sze, S. M. *Physics of Semiconductor Devices*, 2nd ed.; John Wiley & Sons: New York, 1981.

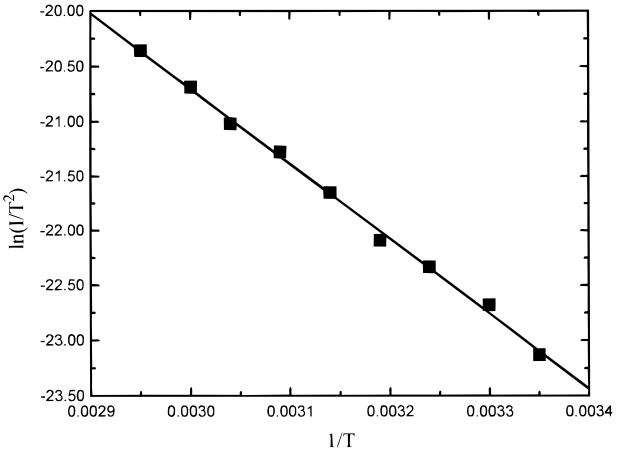

Figure 3. Activation plot for a 7.7 μm Cu_2O film deposited at −0.45 V.

Table 1. Limiting Current as a Function of Temperature for a 10 μm Thick Cu_2O Film

temp (°C)	limiting current (mA/cm^2)	temp (°C)	limiting current (mA/cm^2)
25	0.063	55	0.833
35	0.143	65	1.825
45	0.476		

following equation:

$$\ln(I/T^2) = \ln(A_e A^{**}) - q\phi_B/kT \qquad (1)$$

where I is the current density (A/cm^2), T is the temperature (K), A_e is the electrically active area, A^{**} is the effective Richardson's constant (A/(cm^2 K^2)), q is the elementary charge on the electron ($1.602\ 18 \times 10^{-19}$ C), ϕ_B is the barrier height (eV), and k is Boltzmann's constant ($1.380\ 66 \times 10^{-23}$ J/K). The barrier height can be determined at a set rotation rate (1000 rpm) from the slope of a plot of $\ln(I/T^2)$ versus $1/T$. The slope of the linear region (Figure 3) for a 7.7 μm Cu_2O prelayer on stainless steel equals the activation energy, $q\phi_B/k$, and gives a barrier height value of 0.6 eV. This barrier height between the solution and Cu_2O film is independent of film thickness. Cu_2O also forms a junction with metals, such as copper, with barrier heights between 0.6 and 1.0 eV.[23]

An alternate explanation of the temperature-dependent limiting current would be a CE mechanism, where C represents a homogeneous chemical reaction and E represents an electron transfer at the electrode surface.[31] A slow chemical step (such as ligand dissociation) would generate an electroactive species preceding the electron transfer at the electrode. The rate constant of the chemical step would be temperature dependent and have an activation energy of 0.6 eV.[33]

A practical manifestation of this limiting current is that the solution temperature controls the maximum deposition current density that can be used to deposit copper(I) oxide (see Table 1). For example, if a deposition current density of 1 mA/cm^2 is used, pure copper(I) oxide is deposited at 65 °C, while at 25 °C, the films contain both copper and copper(I) oxide.

Figure 4 compares the linear sweep voltammogram of a stainless steel electrode to steady-state currents at each applied potential for a series of bulk Cu_2O films

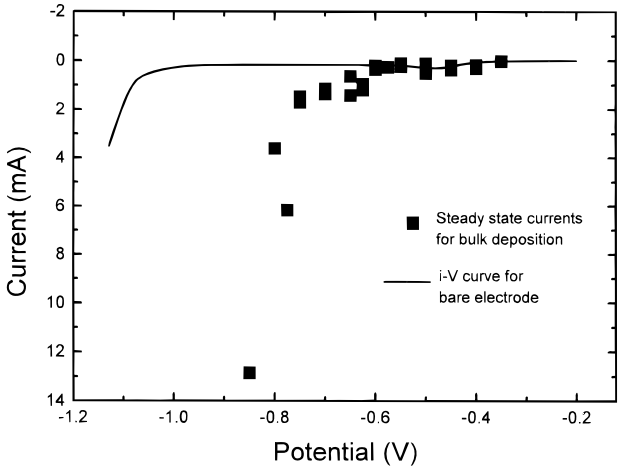

Figure 4. Linear sweep voltammogram (solid line) versus steady state currents (solid squares) for bulk Cu_2O films grown on stainless steel. Scan rate = 10 mV/s.

grown on a stainless steel electrode at 65 °C. At approximately −0.55 V, the steady-state plot deviates from the linear sweep curve. The point where deviation occurs signals the onset of copper deposition in this solution, leaving a 200 mV window for Cu_2O deposition. For the linear sweep curve, as the potential is scanned cathodically, a Cu_2O prelayer forms on the bare stainless steel during this 200 mV window. As the linear sweep continues past −0.55 V, the current still remains low due to the thin Cu_2O layer forming a barrier with the solution. In fact, the linear sweep must be continued past −1.0 V before copper deposition begins on the electrode. If the potential is held in this region of copper deposition for the Cu_2O prelayer, then copper will grow on the electrode in a spiral shape on isolated regions of the electrode. However, when a potential is applied to the bare stainless steel electrode, pure Cu_2O films are only deposited within this 200 mV region. As seen in Figure 4, the steady-state currents (represented as squares) for bulk deposition increase after −0.55 V. If the potential is held between −0.55 and −0.9 V, the resulting films are a mixture of copper and Cu_2O. After −1.0 V, pure copper deposition occurs.

To make sure that the Cu_2O films grown between −0.35 and −0.55 V were single-phase material, Rietveld analysis[34] of a powder from several films grown at 65 °C, −0.45 V and pH 9 was performed on X-ray data collected in the 2θ range 25−85° (Figure 5). A random pattern for analysis was ensured by pulverizing the films, sifting the powder through a 270 mesh sieve, and continually rotating the sample during data acquisition. The solid line is the experimental collected data of X-ray reflections for the powder, while the overlaying crosses are the calculated Rietveld fit. The line below shows the difference pattern between the calculated and experimental patterns. The $Pn\bar{3}$ space group with two formula units per cell was used to calculate the Rietveld fit. The special atomic positions for copper were (0, 0, 0); (0.5, 0.5, 0); (0.5, 0, 0.5); (0, 0.5, 0.5) and for oxygen were (0.75, 0.75, 0.75); (0.25, 0.25, 0.25). A lattice parameter of 0.4266 nm was calculated from the refinement. This lattice parameter gives a Cu−O distance of 0.1847 nm. The final reliability factors from the

(33) The authors wish to acknowledge one of the reviewers for suggesting this alternative mechanism.

(34) Young, R. A. *The Rietveld Method*; Oxford University Press: Oxford, 1995.

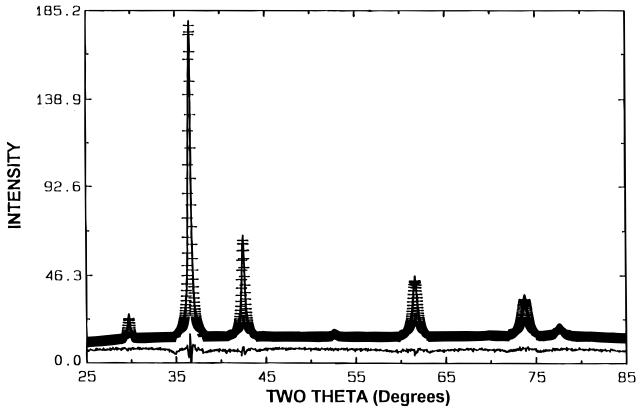

Figure 5. Rietveld analysis for powder produced by grinding several films deposited at 65 °C and $E = -0.45$ V. Powder X-ray data (solid line), Rietveld fit (crosses) and difference pattern (solid line shown below data) are shown for Cu_2O.

Table 2. Reflections, *d* Spacings, and Intensities for the Experimental, Calculated, and JCPDS Card #5-667 for Cu_2O

reflection (*hkl*)	obsd *d* spacing (Å)	obsd intensity I/I_0 (%)	calcd *d* spacing (Å)	calcd intensity I/I_0 (%)	JCPDS *d* spacing (Å)	JCPDS intensity I/I_0 (%)
110	3.020	7	3.020	6	3.020	9
111	2.464	100	2.463	100	2.465	100
200	2.133	37	2.133	36	2.135	37
211	1.742	2	1.742	1	1.743	1
220	1.510	31	1.510	31	1.510	27
311	1.287	22	1.286	25	1.287	17
222	1.232	4	1.232	5	1.233	4
400	1.067	2	1.067	3	1.067	2
331	0.979	4	0.978	5	0.979	4
420	0.954	3	0.954	3	0.954	3
422	0.870	3	0.870	4	0.871	3
511					0.821	3

Rietveld refinement are $R_e = 2.45\%$ and $R_{wp} = 3.88\%$. Table 2 lists the reflections, *d* spacings, and intensities for the experimental and calculated X-ray patterns from the Rietveld analysis. This experimental and calculated data is compared to the JCPDS card file #5-667 for chemically prepared Cu_2O.[35]

The cuprite structure for Cu_2O identified by X-ray diffraction is normally viewed as the copper atom coordinated by two oxygen atoms and each oxygen atom surrounded by a tetrahedron of copper atoms.[36] From this description (shown in Figure 6a) the cuprite structure appears as body-centered cubic. The structure is, however, primitive cubic. This is apparent when the special positions of the atoms are translated by (0.25, 0.25, 0.25). The copper atoms are then at the corners and face of the cubic lattice. The structure for Cu_2O with copper at (0, 0, 0) and oxygen at (0.25, 0.25, 0.25) in Figure 6b shows each oxygen atom surrounded by a tetrahedron of copper atoms.

Films were also analyzed for carbon and hydrogen which may be incorporated into the film from the organic containing solution during deposition.[37] Carbon and hydrogen contents in the Cu_2O films were less than 0.39 and 0.10 wt %, respectively. The very low percentages indicate that the growing films do not incorporate

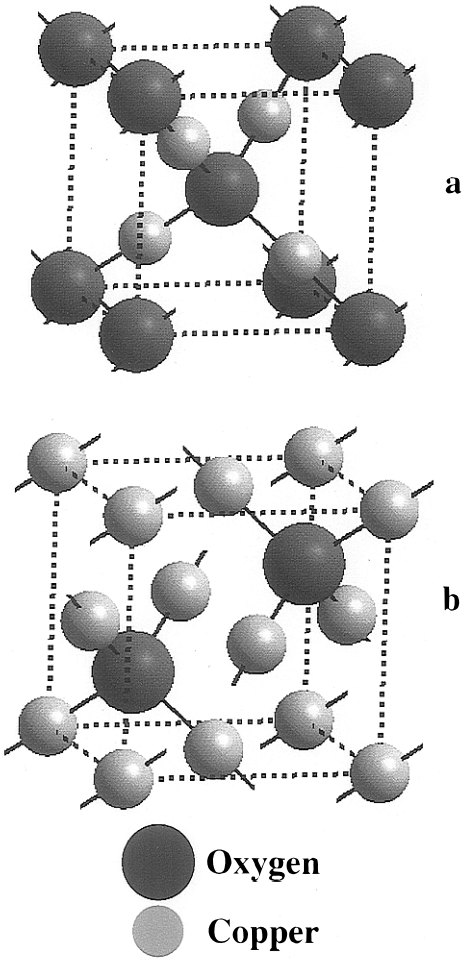

Figure 6. Cuprite structure for Cu_2O. Copper atoms are represented by small light spheres and oxygen atoms are represented by large dark spheres. (a) Copper special positions at (0.25, 0.25, 0.25); (0.75, 0.75, 0.25); (0.75, 0.25, 0.75); (0.25, 0.75, 0.75) and oxygen special positions at (0, 0, 0); (0.5, 0.5, 0.5). (b) Copper special positions at (0, 0, 0); (0.5, 0.5, 0); (0.5, 0, 0.5); (0, 0.5, 0.5) and oxygen special positions at (0.75, 0.75, 0.75); (0.25, 0.25, 0.25).

significant amounts of organic material into the crystal lattice, thus giving pure Cu_2O films.

Figure 7 shows the X-ray diffraction patterns of Cu_2O films deposited at pH 9 and 12. At pH 9, the films have a [100] orientation, while films deposited at pH 12 always showed a [111] orientation. The degree of [111] texture for the films grown at pH 12 increased with applied current density. In all the films grown at pH 12, the intensity of the (111) peak exceeded the value for the JCPDS X-ray card file for a powder of Cu_2O, indicating that the [111] was a preferred orientation and not random. For the pH range 9−13, the deposited films were crystalline. Also films deposited within this pH range from −0.35 to −0.55 V show no X-ray peaks for Cu or CuO.

Grain sizes of the Cu_2O films increased with temperature from an average of 0.5 μm at 25 °C to 3 μm at 65 °C. For both the [100] and [111] orientation, the surface is well-faceted and continuous over the entire substrate. For the [100] oriented Cu_2O, the AFM image reveals four-sided pyramids (Figure 8). The 4-fold symmetry axis is perpendicular to the substrate surface with an average angle of 55° between the sides and top of the crystallites as measured by force goniometry.[38] This

(35) Joint Committee on Powder Diffraction Standards, 1601 Park Lane, Swarthmore, PA 19081.

(36) Burns, G.; Glazer, A. M. *Space Groups for Solid State Scientists*, 2nd ed.; Academic Press: San Diego, 1990.

(37) Cu_2O films were analyzed for carbon and hydrogen content by Quantitative Technologies, Inc.

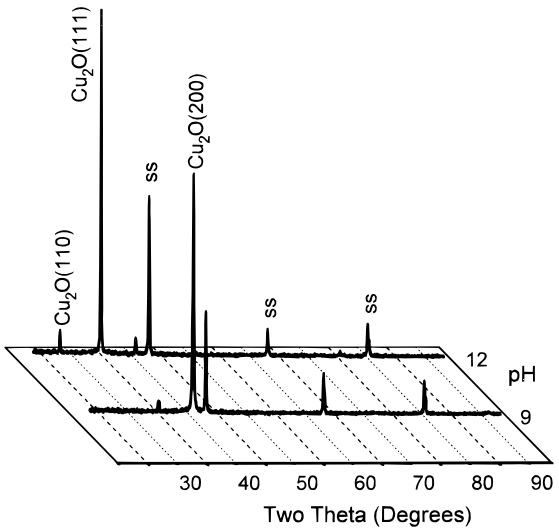

Figure 7. X-ray diffraction patterns of Cu_2O deposited from solutions of pH 9 and 12. The bath temperature is 65 °C and the applied current density is 0.8 mA/cm^2.

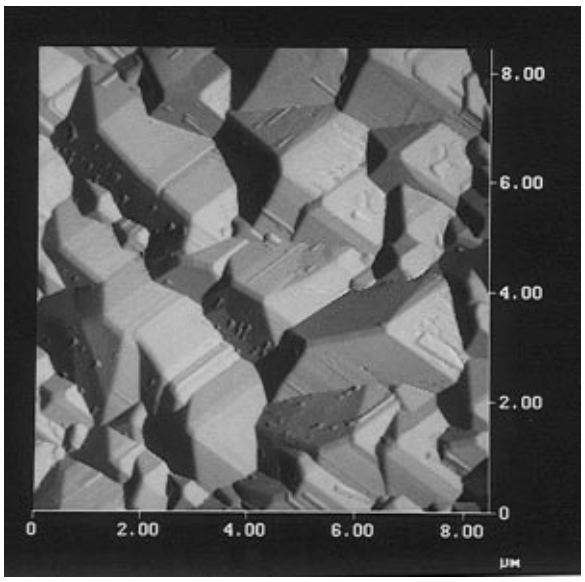

Figure 8. Top-view AFM image of a Cu_2O film deposited at pH 9, $E = -0.45$ V and 65 °C. AFM; z range = 2.5 μm, scan rate = 0.75 Hz.

angle corresponds to the side faces being parallel to the (111) planes and the (100) planes parallel to the substrate surface. The AFM image of a film grown at pH 12 is shown in Figure 9, with a large degree of (111) planes exposed as triangular faces parallel to the substrate.

The electrodeposited films were also characterized optically. Figure 10 shows the reflectance, R, and transmittance, T, spectra of a 6.8 μm thick Cu_2O film. The fringes for both the reflectance and transmittance are caused by constructive and destructive interference between light reflected off the surface of the film and the substrate. These fringes depend on the refractive index and thickness of the film. Thicker films will produce more fringes while thinner films less fringes. These interference maxima and minima can be observed down to a wavelength of about 620 nm in Figure 10. If the thickness of the film is known the index of refraction

(38) Hillier, A. C.; Ward, M. D. *Science* **1994**, *263*, 1261.

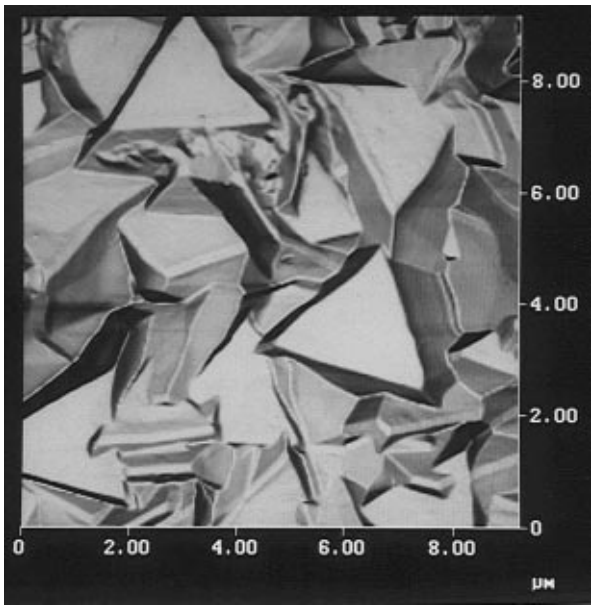

Figure 9. Top-view AFM image of a Cu_2O film deposited at pH 12, $E = -0.45$ V and 65 °C. AFM; z range = 4.2 μm, scan rate = 0.75 Hz.

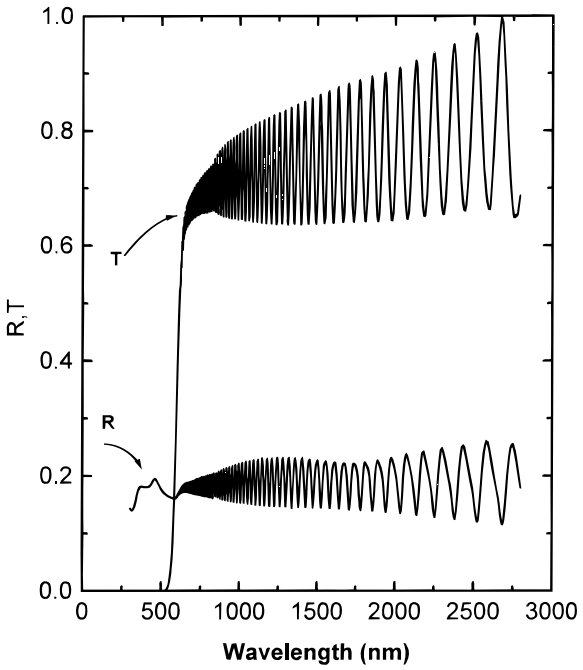

Figure 10. Reflectance (R) and transmittance (T) spectra for a 6.8 μm Cu_2O film as a function of wavelength.

can be calculated from the following equation:[39]

$$n = 1/(1/\lambda_2 - 1/\lambda_1)2x \qquad (2)$$

where n is the index of refraction, x is the thickness of the film (nm), and λ_2 and λ_1 are adjacent minima or maxima (nm) from the transmittance spectrum. A refractive index of 2.6 is determined between wavelengths of 1350 and 2800 nm, where absorption is a minimum in the transmittance spectrum.

The film absorbs strongly at wavelengths below 600 nm. If the thickness, t, is known for the film, then the

(39) Pankove, J. I. *Optical Processes in Semiconductors*; Dover: New York 1971. The equation for calculating the refractive index from the interference fringes in this reference omitted the 2 that appears in the denominator of our eq 2.

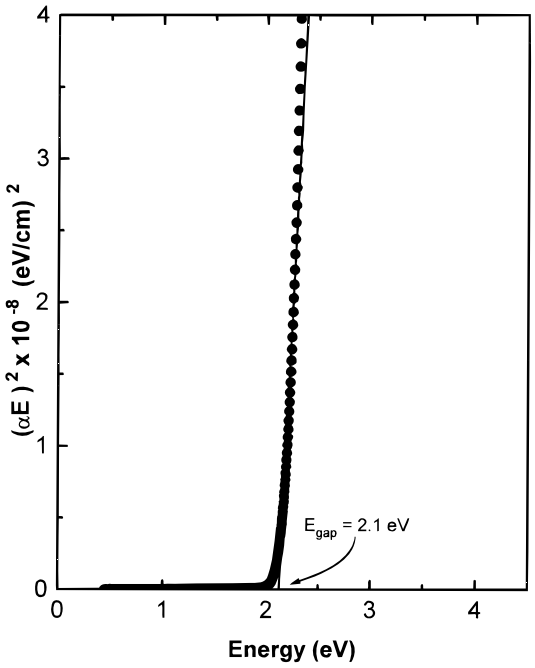

Figure 11. Plot of $(\alpha E)^2$ versus photon energy for a 6.8 μm Cu_2O film. The region between 2.00 and 2.50 is linear and indicates a direct transition. The energy intercept of the linear fit yields a direct bandgap of 2.1 eV.

absorption coefficient, α, can be determined from the following simplified equation:[39]

$$e^{-\alpha t} = T/(1 - R)^2 \qquad (3)$$

where R and T are the reflectance and transmittance of the film. The type of transition is then determined by a plot of either $\alpha^{1/2}$ or $(\alpha E)^2$ versus the energy of the photons, E. If $(\alpha E)^2$ versus E is linear, then the transition is direct, and if $\alpha^{1/2}$ versus E is linear, then the transition is indirect.[16,39] The plot of $(\alpha E)^2$ versus E is linear as shown in Figure 11, therefore the transition is direct. The x intercept of the plot gives the direct bandgap value, E_g, of 2.1 eV for the electrochemically deposited Cu_2O.

An energy level diagram consistent with our bandgap and barrier height measurements is shown in Figure 12. Copper(I) oxide is a p-type semiconductor with a direct bandgap of 2.1 eV. The cathodic deposition current is limited by a rectifying contact at the semiconductor/solution interface with a barrier height of 0.6 eV. We have shown that the limiting current is strongly temperature dependent. It increases from 8 μA at 25 °C to 230 μA at 65 °C. Although Figure 12 suggests

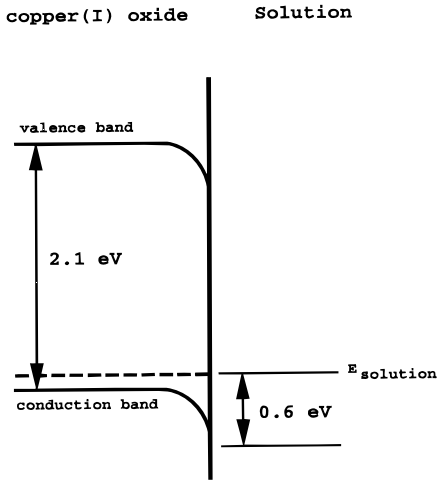

Figure 12. Proposed energy-level diagram for copper(I) oxide/solution interface.

that this 0.6 eV barrier is due to an energetic mismatch between the semiconductor Fermi level and the solution potential, our measurements do not give us insight into the mechanism of barrier formation. More detailed work will be required to determine whether other effects, such as surface states, may be inducing the barrier. We also plan to determine whether the electrical properties of the copper(I) oxide can be tuned by varying the deposition potential.

Conclusions

Cuprous oxide films are electrodeposited onto various substrates from an alkaline copper(II) lactate solution. A Schottky-like rectifying barrier of 0.6 eV forms at the semiconductor/solution interface. This barrier height is determined from the exponential dependence of the deposition current with the solution temperature. Films of preferred orientation are deposited, with [100] deposited at pH 9 and [111] deposited at pH 12. AFM images of the cuprous oxide show the [100] oriented films arranged as four-sided pyramids, while the [111] oriented films have triangular crystals. Reflectance and transmittance of the electrodeposited films give a direct bandgap of 2.1 eV.

Acknowledgment. This work was supported by National Science Foundation Grant DMR-9202872, Office of Naval Research Grant No. N00014-94-1-0917, and the University of Missouri Research Board.

CM9602095